Journal of Catalysis 266 (2009) 145–155

Contents lists available at ScienceDirect

Journal of Catalysis

journal homepage: www.elsevier.com/locate/jcat

Microkinetic analysis of the epoxidation of styrene catalyzed by (porphyrin)Mn encapsulated in molecular squares

Gloria A.E. Oxford [a], María C. Curet-Arana [a,b], Debarshi Majumder [a], Richard W. Gurney [c,d], Melissa L. Merlau [c], SonBinh T. Nguyen [c], Randall Q. Snurr [a], Linda J. Broadbelt [a,*]

[a] Department of Chemical and Biological Engineering, Northwestern University, 2145 Sheridan Road, Evanston, IL 60208, United States
[b] Department of Chemical Engineering, University of Puerto Rico, Mayagüez, Puerto Rico
[c] Department of Chemistry, Northwestern University, 2145 Sheridan Road, Evanston, IL 60208, United States
[d] Department of Chemistry, Simmons College, 300 The Fenway, Boston, MA 02115, United States

ARTICLE INFO

Article history:
Received 13 March 2009
Revised 3 June 2009
Accepted 4 June 2009

Keywords:
(Porphyrin)Mn
Epoxidation
Styrene
Molecular squares
Microkinetic modeling
Oxidation
Biomimetic catalysis

ABSTRACT

Experiments and microkinetic modeling were used to investigate the kinetics of styrene epoxidation catalyzed by (porphyrin)Mn using iodosylbenzene. While the kinetics follow the general form of Michaelis–Menten rate expressions as proposed in the literature, these simplified rate forms cannot capture all the details of the kinetics simultaneously, most notably catalyst deactivation. In contrast, a microkinetic model based on elementary steps, including deactivation via μ-oxo dimer formation and irreversible degradation, is able to capture experimental data over all reaction times and for different (porphyrin)Mn. Experimentally, we show that encapsulation of (porphyrin)Mn in a supramolecular cavity known as a molecular square significantly reduces catalyst deactivation, which is in agreement with previous experimental studies. Microkinetic modeling also captured the kinetics of this system. Net rate analysis revealed that production of epoxide was primarily due to encapsulated catalysts, and the model was able to quantify the difference in the concentration of deactivated catalyst with and without encapsulation.
© 2009 Elsevier Inc. All rights reserved.

1. Introduction

Inspired by the high stability and selectivity of enzymes, much research has been devoted to developing synthetic biomimetic catalysts. In particular, synthetic metalloporphyrins have been utilized by many researchers in olefin epoxidation to mimic cytochrome P-450, which has an iron porphyrin active site. Groves et al. [1] first demonstrated that (porphyrin)Mn was an active catalyst for epoxidation reactions. Since then, significant effort has been focused on elucidating the catalytic mechanism. Current opinion favors a metal-oxo species as the active epoxidizing intermediate, and oxygen transfer to the olefin involves a two-electron reduction of the metal complex [2]. A complete description of the reaction mechanism, however, has been complicated by the rapid deactivation of (porphyrin)Mn under reaction conditions. Nolte and coworkers [3–5] have cautioned about the influence of μ-oxo dimerization, in particular, on kinetic analysis.

To enhance the catalyst stability, researchers have tried to isolate the catalytic center using a variety of methods [6]. A significant improvement in the stability of metalloporphyrins was achieved by immobilizing them onto a solid support, such as silica [7–9]. More elaborate structures, such as the well-known picnic-basket porphyrins created by Collman's group [10], have also improved the stability of porphyrins. However, the synthesis of some of these structures is time-consuming, and they are still vulnerable to degradation. Another strategy is to encapsulate the porphyrin in the cavity of a metallocyclophane (a "molecular square"). This bio-inspired approach aims to create a protein-like structure that extends the life of the catalyst and enhances its selectivity [11]. Molecular squares (MS) can be formed with rhenium atoms in the corners and zinc porphyrin ligands on the sides [12–14], and these structures can encapsulate (porphyrin)Mn as shown in Fig. 1. Experiments have indicated that by using millimolar solutions of the square complex and of the catalyst 2,8,12,18-tetrabutyl-3,7,13,17-tetramethyl-5,15-*bis*(4-pyridyl)porphyrinato manganese(III) chloride (MnDPyP) (Fig. 1), a 10-fold increase in the turnover number is produced. Also, the stability of MnDPyP was significantly increased since the catalyst was active 3 h longer than the non-encapsulated MnDPyP [15]. Nevertheless, the stability of the structure depends on the binding strength of the catalyst within the cavity. Results have indicated that approximately 3% of the catalyst remains unbound, and after 3 h of reaction, all of the catalyst is destroyed. While catalyst stability is enhanced by encapsulation or other immobilization techniques, the kinetics are altered and cannot be measured accurately.

Because of the uncertainty over the reaction mechanism and the effect of catalyst deactivation, a comprehensive modeling

* Corresponding author. Fax: +1 847 491 3728.
E-mail address: broadbelt@northwestern.edu (L.J. Broadbelt).

0021-9517/$ - see front matter © 2009 Elsevier Inc. All rights reserved.
doi:10.1016/j.jcat.2009.06.003

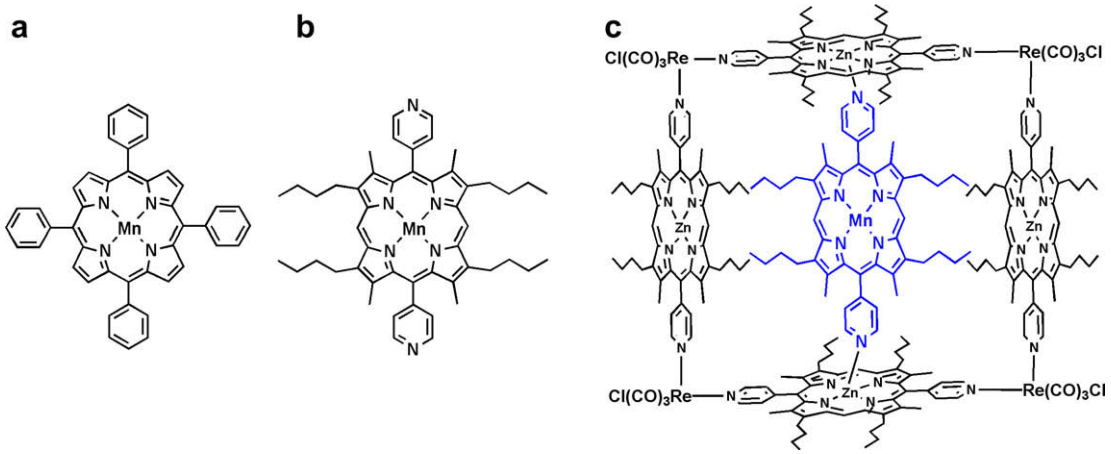

Fig. 1. Mn–porphyrin complexes studied: (a) MnTPP, (b) MnDPyP, and (c) MnDPyP encapsulated in molecular squares.

approach to study reaction kinetics would greatly add to the current understanding of the (porphyrin)Mn system. Microkinetic analysis is a powerful tool for studying a reaction mechanism without making any simplifying assumptions about the rate-determining step. In microkinetic analysis, the overall rate of the reaction is obtained by considering all the elementary steps in the catalytic reaction explicitly and by solving the reactor design equations derived for each species in the reaction mechanism [16]. Comparison of microkinetic modeling results based on different postulated mechanisms with experimental data can reveal the catalytic mechanism. Further probing of the model can provide detailed insight into various aspects of the mechanism, such as identifying intermediate species that cannot be characterized experimentally, the rate-determining step, and the effect of deactivation. To date, this type of modeling approach has not been utilized in the study of these complex catalytic systems.

Using kinetic data and microkinetic modeling, we propose a mechanism of olefin epoxidation by MnDPyP that is able to capture data over a wide range of concentrations and reaction times, including cases where catalyst deactivation is significant. We show that the mechanism can be applied to other porphyrin systems, specifically to 5,10,15,20-tetraphenyl-21*H*,23*H*-porphine manganese(III) chloride (MnTPP) (Fig. 1), and capture experimental data well. The proposed mechanism was then expanded to account for catalysis by encapsulated porphyrins, namely for MnDPyP encapsulated in molecular squares ([MnDPyP·MS]), and experimental data for this system are also described well. Importantly, the microkinetic analysis quantifies the impact of deactivation on the kinetic data and gives insight into the nature of the rate-determining step. The results of the detailed microkinetic model are then consolidated to show how Michaelis–Menten kinetics are obeyed at short reaction times, in agreement with a number of experimental studies [17–22], although the true kinetics are more complex than the simple Michaelis–Menten kinetics. Our results also capture the significant decrease in catalyst deactivation observed by encapsulation of MnDPyP in MS, and show that the MS do not simply act as a reservoir of catalyst. Microkinetic modeling allowed us to answer questions about the reaction mechanism not easily accessible by experiments alone.

2. Methods

2.1. Experimental

Iodosylbenzene was synthesized by adding NaOH (3 N, 150 mL) to iodosylbenzene diacetate (0.10 mol) in a 250-mL beaker while stirring for 1 h. The solid iodosylbenzene was filtered, washed twice with water (200 mL), and dried under aspiration. The residue was then washed with dichloromethane (75 mL) and dried under aspiration. MnTPP was purchased from Aldrich and was used as received. MnDPyP was prepared from the reaction of free-base dipyridyl porphyrin with $MnCl_2{\cdot}4H_2O$ as described by Adler et al. [23]. MS were synthesized as described by Slone and Hupp [24]. Styrene, octane, which was used as an internal standard, and dichloromethane, which served as the solvent, were purchased from Aldrich.

Kinetic experiments were performed in constant temperature batch reactions. The catalyst was added to a round-bottomed flask containing a magnetic stir bar. The MS were also added at this point into the [MnDPyP·MS] system. Octane (internal GC standard, 0.03 M), styrene, and dichloromethane were added to the flask, which was then sealed to avoid evaporation. The flask was kept under stirring until the desired temperature (25 °C) was reached. The temperature was maintained by a water bath and controlled using a Cole-Parmer 04644 Series digital magnetic stirrer and temperature controller. To start the reaction, solid iodosylbenzene was added to the reaction flask. Agitation of the system was maintained at 350 rpm throughout the experiments. This stirring rate was determined to give similar concentration profiles as stirring rates of 150 rpm and 500 rpm. Samples (40 μL) were taken periodically and filtered through a plug of 0.40 g of silica gel and glass fiber to remove the catalyst. The filter was washed with dichloromethane (2 × 1 mL), and the filtrates were combined for quantitative GC analysis. Gas chromatographic analyses of reactant and product concentrations were performed on a Hewlett-Packard GC 6890 Series fitted with an HP-5 column. All experiments were performed at least twice. Error bars on the graphs correspond to the standard deviation among the replicates for each particular time.

The ranges of the initial styrene and catalyst concentrations are given in Table 1. The initial iodosylbenzene concentration was 0.1 M in all experiments. In the MnTPP experiments, 5.0 mL and 15.0 mL reaction volumes were used for the initial catalyst concentrations of 0.1 mM and 0.045 mM, respectively. A reaction volume of 7.0 mL was used when the initial MnDPyP concentration was 0.05 mM in the [MnDPyP·MS] system. In all other experiments, the reaction volume was 3.0 mL.

2.2. Modeling

2.2.1. Selection of model

A reaction mechanism for non-encapsulated catalysts (Fig. 2a) was proposed based on the literature and on quantum mechanics/molecular mechanics (QM/MM) calculations of the potential

Table 1
Range of initial concentrations for the kinetics experiments.

System	Concentration range for styrene (M)	Concentration range for catalyst (mM)	Concentration range for MS (mM)
MnTPP	0.05–1.0	0.045–1.1	N/A
MnDPyP	0.05–0.5	0.2–1.0	N/A
[MnDPyP·MS]	0.05–1.0	0.045–0.8	0.2–2.0

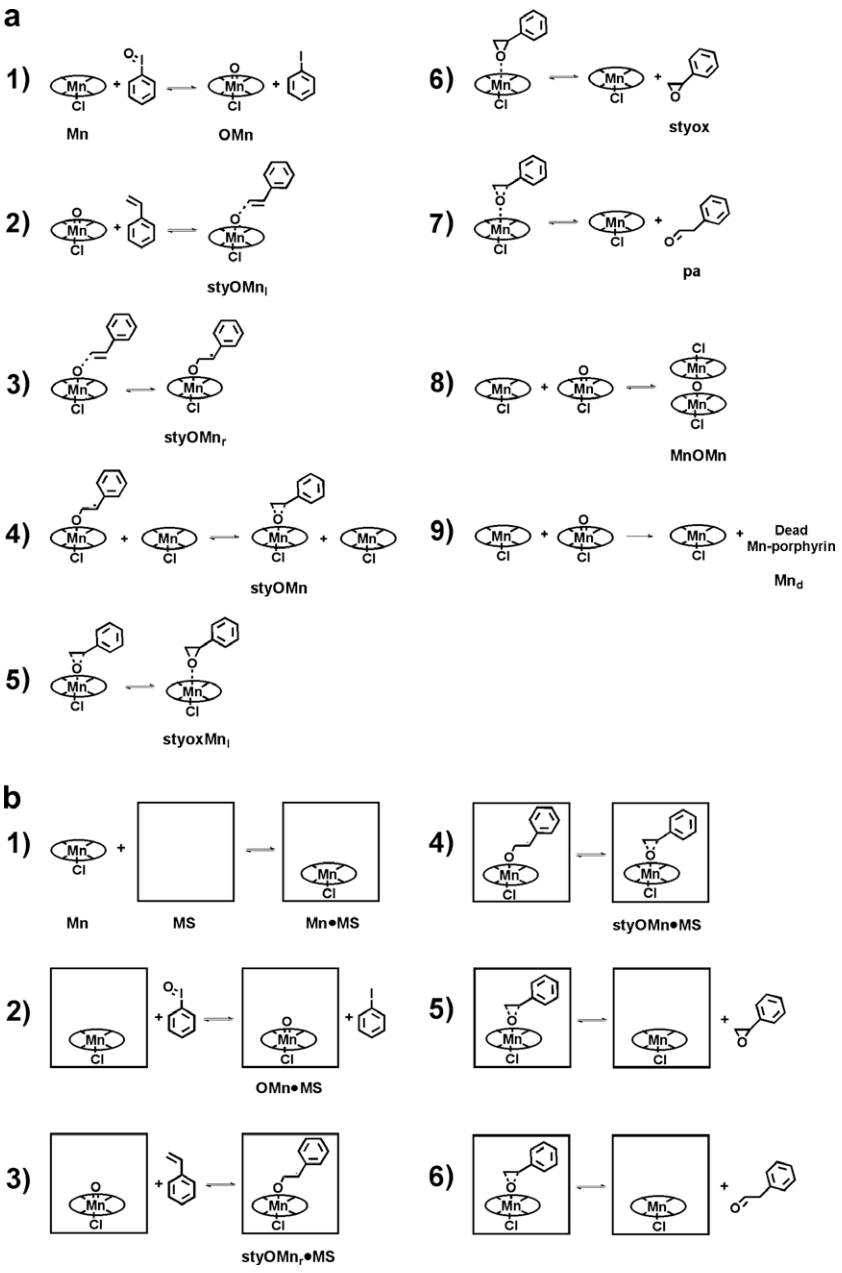

Fig. 2. Proposed reaction mechanisms for the epoxidation of styrene catalyzed by (a) MnTPP and MnDPyP and (b) encapsulated MnDPyP.

energy surface for epoxidation of styrene by a model (porphyrin)Mn [25,26]. In Step 1, the (porphyrin)Mn is oxidized to the Mn^V-oxo (Mn^V = O, **OMn** in Fig. 2a). In the literature, this species was formed by oxidation of (porphyrin)Mn with *m*-CPBA, HSO_5^-, and ClO^-, and was characterized with UV–vis and ^1H NMR by Groves and coworkers [27–29]. Laser flash photolysis has also been used to generate Mn^V-oxo complexes, which were further characterized with UV–vis [30]. These complexes were shown to be the major epoxidizing intermediates in the epoxidation of *cis*-stilbene by iodosylbenzene. Nam and coworkers [31] characterized Mn^V-oxo species with UV–vis, EPR, resonance Raman, and X-ray absorption spectroscopy. However, they found the Mn^V-oxo species to have low reactivity with olefins. The Mn^V-oxo species has also been detected with electrospray mass spectrometry in the closely related (salen)Mn system, where it was shown to be reactive with alkenes and sulfides [32,33]. It should be noted that Groves and

coworkers have proposed that a Mn^{IV}-oxo species also participates in the epoxidation of alkenes, leading to non-stereospecificity in the products [34,35].

The Mn^{V}-oxo species (**OMn**) then forms a loosely bound complex with styrene (**styOMn$_l$**, Step 2 in Fig. 2a), which was found with QM/MM calculations [25]. The loosely bound complex **styOMn$_l$** reacts to form a radical intermediate (**styOMn$_r$**, Step 3). In the literature, the complex between **OMn** and the olefin has been proposed to be a carbon radical, metallaoxetane species, carbocation, or π-radical cation based on kinetic studies. (Porphyrin)Mn-catalyzed epoxidation has also been suggested to occur through a concerted mechanism [3,4,17,20,36]. However, there exists no direct evidence as to which intermediate plays a role in the reaction mechanism. Recent computational studies to map the potential energy surface with QM/MM calculations found the radical intermediate to be most likely [25,26]. Full DFT calculations of the potential energy surface in (salen)Mn-catalyzed epoxidation also determined the radical intermediate to be the most favorable intermediate [37–39].

The reaction proceeds with the transformation of the radical intermediate (**styOMn$_r$**) into the product complex (**styOMn**, Step 4 in Fig. 2a). The product complex **styOMn** forms a second product complex (Step 5), which we refer to as the loosely bound product, **styoxMn$_l$**. These two species were found by QM/MM calculations in an investigation of the reaction coordinate [25]. This loosely bound product **styoxMn$_l$** dissociates to give styrene oxide (**styox**) and the catalyst (Step 6). The product complex may also react to form phenylacetaldehyde (**pa**) and catalyst (Step 7). The final two steps represent μ-oxo dimer formation (**MnOMn**) and complete deactivation of the catalyst to form dead catalyst, **Mn$_d$**. Dimerization of (porphyrin)Mn is a well-known mode of deactivation [3–5]. It was assumed that the non-encapsulated MnDPyP and MnTPP systems could be described by the same mechanism. For the mechanism shown in Fig. 2a, 13 differential equations were used, one for each of the individual species.

The [MnDPyP·MS] system involved a combination of catalyses by the free catalyst and by the encapsulated catalyst. The mechanism for this system therefore included the mechanism shown in Fig. 2a for the non-encapsulated MnDPyP and the additional elementary steps shown in Fig. 2b. For the [MnDPyP·MS] system, a total of 18 differential equations were solved. The solutions to these differential equations were obtained using the differential equation integrator DDASAC [40].

2.2.2. Microkinetic modeling

In the microkinetic model, the rate constants and equilibrium constants need to be specified for each elementary step, and ranges were fixed based on quantum chemical calculations when possible. Equilibrium constants for each of the elementary steps were calculated based on the free energies obtained from QM/MM calculations [25] as described in Eq. (1)

$$K = (c^0)^{1-n} \exp\left(\frac{-\Delta G}{RT}\right) = \frac{k_f}{k_r} \tag{1}$$

where ΔG is the difference in free energy between the products and the reactants, c^0 is a standard state concentration to which the quantum chemical calculations are referenced and that is calculated using the ideal gas law, n is the molecularity of the reaction, and k_f and k_r are the forward and reverse rate constants, respectively. Rate constants derived from quantum mechanical calculations and transition state theory were estimated using Eq. (2)

$$k = \left(\frac{k_B T}{h}\right)\kappa(T)(c^0)^{1-n} \exp\left(\frac{-\Delta G^{\neq}}{RT}\right) \tag{2}$$

where $\Delta G^{\neq}$ is the difference in free energy between the transition state and the reactants, k_B and h are Boltzmann's and Planck's constants, respectively, and $\kappa(T)$ is a correction factor for quantum mechanical tunneling that was added in order to take into account the possibility that a particle can penetrate the reaction barrier without passing through the activated complex. The Wigner correction was used to estimate this parameter [41]:

$$\kappa(T) = 1 + \frac{1}{24}\left(1.44\frac{v_i}{T}\right)^2 \tag{3}$$

where v_i is the value of the imaginary vibrational frequency at the transition state in cm^{-1}, and T is the temperature in K. The correction factor had a value of 1.07 for the formation of the radical intermediate (Step 3 in Fig. 2a) and of 1.16 for the formation of the product complex (Step 4).

Using the quantum chemical values as initial guesses, the forward rate parameters and the equilibrium constants were optimized within the error of the QM/MM calculations (±15 kJ/mol for the free energy) by performing least squares regression, while the reverse rate constants were fixed by the values of k_f and the equilibrium constants [42,43]. A hybrid scheme with a genetic algorithm (GA) [44] as a stochastic global optimizer and a gradient-based local optimizer (GREG) [45] was used to optimize all the parameters. For each system, 20 jobs were run with five iterations of the hybrid GA–GREG scheme. In the GA run, the crossover probability was 0.8 in all cases. The arithmetic-, heuristic- and simple-crossover probabilities were set to 0.1, 0.95, and 1.0, allowing a significant amount of extrapolation inside the parametric space. The probability to undergo mutation was set to 0.1 in the MnTPP system and to 0.2 in the other two systems. The probabilities of boundary-, gauss-, non-uniform-, and uniform-mutations were set at 0.2, 0.8, 0.9, and 1.0, respectively. Elitism was applied by preserving the top 5% of individuals in the next generation. A complete description of these operators can be found in the book by Goldberg [44]. For MnTPP, a total of 324 experimental data points were used. For non-encapsulated MnDPyP and [MnDPyP·MS], 112 and 210 data points were used, respectively. All rate parameters were optimized in the MnTPP and MnDPyP systems. The optimized parameters for the non-encapsulated MnDPyP were used in the microkinetic modeling of [MnDPyP·MS], and only the forward and reverse rate constants for the steps shown in Fig. 2b were optimized. The equilibrium binding constant K_b of Step 1 shown in Fig. 2b was fixed at $1.0 \times 10^6\ M^{-1}$ based on the experimental results of Merlau et al. [15]. Because quantum chemical values were not available for chemistry inside the MS, small lower bounds were set, and the upper bounds were fixed based on reasonable upper limits for unimolecular and bimolecular rate constants [46]. The lower bound on all rate constants for the chemistry inside the MS in the [MnDPyP·MS] system was 1.0×10^{-5} (s^{-1} or $M^{-1}\ s^{-1}$). The upper bound on rate constants for unimolecular reactions was $1.0 \times 10^{12}\ s^{-1}$, while the upper bound for bimolecular reactions was $1.0 \times 10^{10}\ M^{-1}\ s^{-1}$.

3. Results and discussion

3.1. Non-encapsulated MnDPyP

At short reaction times, a Michaelis–Menten relationship has been found to describe kinetic data by a number of groups [17–20,22] with the catalyst concentration specified to be a constant at its initial value. This relationship fails at long reaction times, however, due to the presence of deactivation that causes a decrease in the porphyrin concentration as the reaction proceeds. As shown in Fig. 3, the experimentally determined reaction rate for the MnDPyP system decreased significantly at longer times even though the maximum conversion ranged

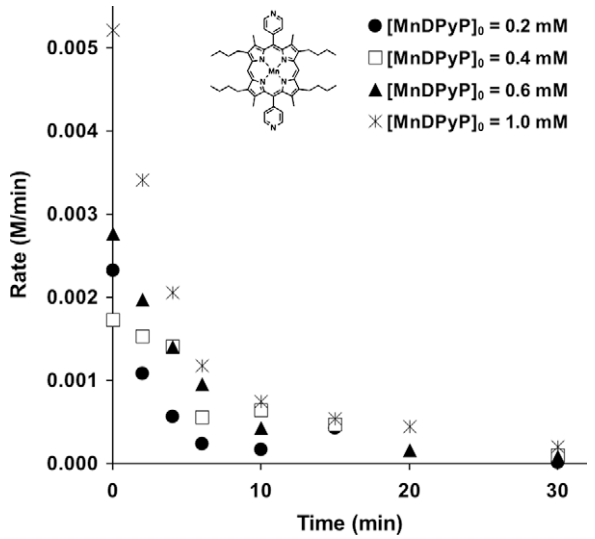

Fig. 3. Experimental reaction rates vs. time for the epoxidation of styrene using various initial MnDPyP (structure shown in the inset) concentrations with $[\text{styrene}]_0 = 0.3$ M and $[\text{iodosylbenzene}]_0 = 0.1$ M.

from only 12% to 36% with increasing initial catalyst concentrations. Based on the typical rate expression for Michaelis–Menten kinetics

$$V_{\text{obs}} = \frac{V_{\max}[S]}{K_{\text{m}} + [S]} \tag{4}$$

where $V_{\max}$ is proportional to $[\text{MnDPyP}]_0$, K_{m} is a binding constant, and $[S]$ is the substrate concentration, the observed rate, V_{obs}, should still be non-zero at such low conversions. Given the dramatic changes in and the pronounced flattening of the rate at times as short as 5 min shown in Fig. 3, it was not surprising that our attempts to capture the data at all times using the rate expression in Eq. (4) were unsuccessful. One possible patch for the rate expression in Eq. (4) is to express the concentration of MnDPyP using an analytical expression to account for μ-oxo dimer formation (see Ref. [4]) and complete deactivation of the catalyst, but it is unclear what the form of this expression should be, especially since the concentration of MnDPyP has some dependence on the styrene concentration. A microkinetic model is thus an attractive alternative that includes these deactivation steps at a mechanistic level, and therefore should be able to capture the kinetic data at all times.

In formulating a microkinetic model, it is necessary to postulate a mechanism, but experimental efforts and quantum chemical calculations provided a limited number of reasonable candidates. A number of mechanisms were tested, and the mechanism shown in Fig. 2a was determined to fit the data the best based on the sum of squared error [47]. A simple base case mechanism gleaned from the literature consisted of the oxidation of the (porphyrin)Mn to **OMn**, formation of **styOMn$_r$**, steps for the formation of styrene oxide and phenylacetaldehyde from **styOMn$_r$**, μ-oxo dimerization, and deactivation. This simple mechanism, however, was not able to fit the experimental data well. Importantly, the dependence of the rate on the catalyst concentration was not captured well, and the rate was not retarded sufficiently at longer times. The key changes from this basic mechanism that allowed all the data to be captured well were the inclusion of two different forms of the olefin-oxidant complex (i.e., **styOMn$_r$** and **styOMnI**) as revealed by the QM/MM calculations of Curet-Arana et al. [26] and the addition of the second-order dependence on MnDPyP in Step 4 shown in Fig. 2a. There is some precedence in related oxidation literature for a bimolecular step involving the catalyst [48], although the mode of interaction of the free catalyst with the oxidized intermediate is unknown.

Comparisons of the experimental and model concentration profiles of styrene oxide for all MnDPyP data collected are shown in Fig. 4 (see Supplementary material for phenylacetaldehyde concentration profiles). The optimized rate parameters from the microkinetic model that achieve this agreement with a best sum of squared error of 7.12×10^{-5} M^2 are given in Table 2. The agreement is very good for all reaction times for various initial MnDPyP concentrations and an initial styrene concentration of 0.3 M (Fig. 4a). The calculated profiles from the model showed good agreement within the error of the experiments (see Supplementary material). The model also does a good job of capturing data for a range of initial styrene concentrations and an initial MnDPyP concentration of 0.2 mM (Fig. 4b). The styrene oxide and phenylacetaldehyde concentrations are slightly underpredicted at long reaction times for initial styrene concentrations of 0.1 and 0.3 M, but the general trends are clearly captured. The microkinetic model captured the selectivity of the MnDPyP catalyst, with a calculated selectivity of approximately 70% favoring styrene oxide at all times and under all conditions studied, which was the same selectivity

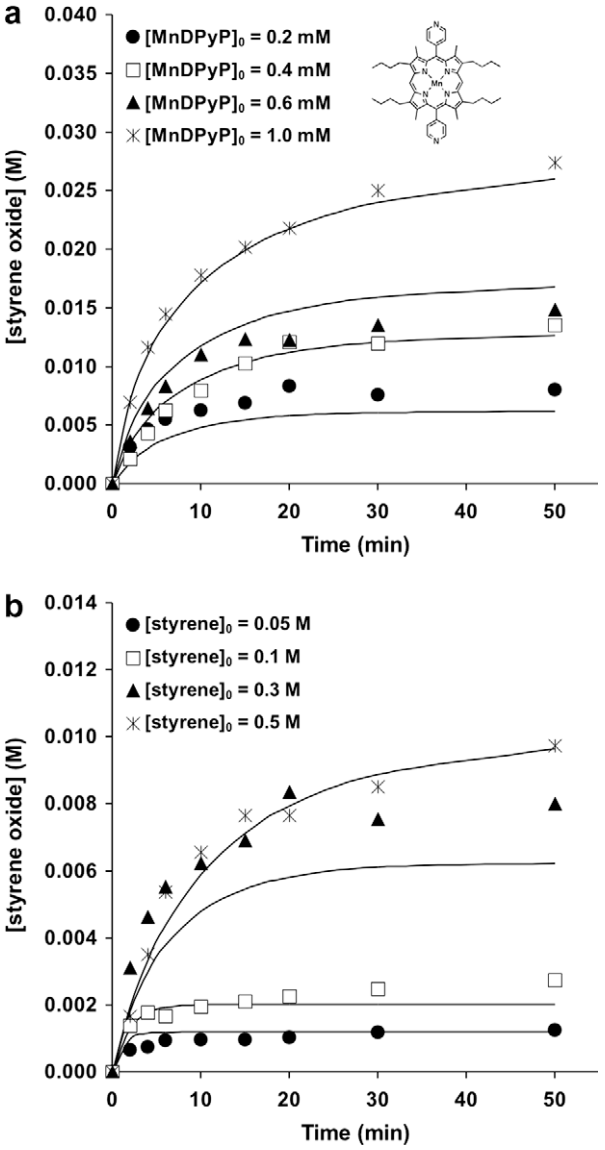

Fig. 4. Styrene oxide concentration profiles for (a) various initial MnDPyP (structure shown in the inset) concentrations with $[\text{styrene}]_0 = 0.3$ M and (b) various initial styrene concentrations with $[\text{MnDPyP}]_0 = 0.2$ mM. In all cases, $[\text{iodosylbenzene}]_0 = 0.1$ M. Symbols represent experimental data, and microkinetic model results are represented with lines.

Table 2
Rate constants and equilibrium constants for the reaction mechanism shown in Fig. 2. Comparison of parameters as obtained with the QM/MM method and after their optimization against experimental data is provided for the MnDPyP system. Mn = MnDPyP; PhIO = iodosylbenzene; OMn = DPyPMnO; styOMn$_1$ = loosely bound reactant; styOMn$_r$ = radical intermediate; styOMn = fully formed product complex; styoxMn$_1$ = loosely bound product; styox = styrene oxide, pa = phenylacetaldehyde; MnOMn = μ-oxo (porphyrin)Mn dimer; and Mn$_d$ = dead catalyst. Limits for the optimizations when theoretical values were available: $K_{QM/MM}$ (or $k_{QM/MM}$) × 425 (upper limit) and $K_{QM/MM}$ (or $k_{QM/MM}$) × 0.002 (lower limit). This corresponds to ±15 kJ/mol in ΔG or $\Delta G^{\neq}$.

Step	Reaction and rate equation	QM/MM initial guesses	Optimized parameters
1	Mn + PhIO ↔ OMn + PhI		$k_{f1} = 1.43\ M^{-1}\ s^{-1}$
	$r_1 = k_{f1}[Mn][PhIO] - k_{r1}[OMn][PhI]$		$k_{r1} = 1.00 \times 10^{-20}\ M^{-1}\ s^{-1}$
2	OMn + sty ↔ styOMn$_l$		$k_{f2} = 1.70 \times 10^{9}\ M^{-1}\ s^{-1}$
	$r_2 = k_{f2}[OMn][sty] - k_{f2}/K_2[styMnO_l]$	$K_2 = 1.71 \times 10^{1}\ M^{-1}$	$K_2 = 1.56 \times 10^{2}\ M^{-1}$
3	styOMn$_l$ ↔ styOMn$_r$	$k_{f3} = 4.68 \times 10^{2}\ s^{-1}$	$k_{f3} = 1.05 \times 10^{4}\ s^{-1}$
	$r_3 = k_{f3}[styOMn_l] - k_{f3}/K_3[styOMn_r]$	$K_3 = 3.64 \times 10^{-4}$	$K_3 = 1.28 \times 10^{-1}$
4	styOMn$_r$ + [Mn] ↔ styOMn + [Mn]	$k_{f4} = 3.84 \times 10^{9}\ M^{-1}\ s^{-1}$	$k_{f4} = 1.77 \times 10^{7}\ M^{-1}\ s^{-1}$
	$r_4 = k_{f4}[styOMn_r][Mn] - k_{f4}/K_4[styOMn][Mn]$	$K_4 = 1.06 \times 10^{5}$	$K_4 = 1.50 \times 10^{6}$
5	styOMn ↔ styoxMn$_l$		$k_{f5} = 3.53 \times 10^{5}\ s^{-1}$
	$r_5 = k_{f5}[styOMn] - k_{f5}/K_5[styoxMn_l]$	$K_5 = 2.04 \times 10^{9}$	$K_5 = 3.24 \times 10^{7}$
6	styoxMn$_l$ ↔ Mn + styox	$k_{f6} = 1.76 \times 10^{11}\ s^{-1}$	$k_{f6} = 7.45 \times 10^{13}\ s^{-1}$
	$r_6 = k_{f6}[styoxMn_l] - k_{f6}/K_6[Mn][styox]$	$K_6 = 1.30 \times 10^{-3}\ M$	$K_6 = 1.32 \times 10^{-2}\ M$
7	styOMn ↔ Mn + pa		$k_{f7} = 1.50 \times 10^{5}\ s^{-1}$
	$r_7 = k_{f7}[styOMn] - k_{f7}/K_7[Mn][pa]$	$K_7 = 3.44 \times 10^{29}\ M$	$K_7 = 1.46 \times 10^{32}\ M$
8	Mn + OMn ↔ MnOMn		$k_{f8} = 1.11 \times 10^{6}\ M^{-1}\ s^{-1}$
	$r_8 = k_{f8}[Mn][OMn] - k_{f8}/K_8[MnOMn]$	$K_8 = 1.24 \times 10^{19}\ M^{-1}$	$K_8 = 2.95 \times 10^{16}\ M^{-1}$
9	Mn + OMn → Mn$_d$ + Mn		$k_{f9} = 2.87 \times 10^{5}\ M^{-1}\ s^{-1}$
	$r_9 = k_{f9}[Mn][OMn]$		

determined experimentally. The overall ability of the microkinetic model to describe the kinetics of the MnDPyP system was very good.

Deactivation played a significant role in the kinetics of the MnDPyP system. With decreasing initial styrene concentrations, the fraction of catalyst in inactive form increased as quantified by the microkinetic model (Fig. 5a). In this system, most of the inactive catalyst was found in μ-oxo dimer form (Fig. 5b), whose formation was favored by a larger forward rate constant ($k_{f8} > k_{f9}$) and a large equilibrium constant. Approximately 11% of the inactive catalyst was completely dead in the MnDPyP system under all conditions studied. The catalyst was found to be essentially completely deactivated after 6 min at an initial styrene concentration of 0.05 M. Even at a higher initial styrene concentration of 0.3 M, the catalyst was 30% deactivated after 2 min and almost 80% deactivated after 10 min. The microkinetic model illustrates how significant the deactivation of the catalyst is, and serves to explain why the Michaelis–Menten relationship proposed in the literature [17–20,22] based on a constant catalyst concentration cannot be fitted to the data at long reaction times.

The rate-determining step for the MnDPyP system was investigated using the model. In the literature, two steps have been proposed as the rate-determining steps: the oxidation of the (porphyrin)Mn to **OMn** [3,49] and the oxygen transfer to the olefin [17,22]. Experimental studies to date have not clearly established the nature of the rate-determining step. To ascertain the rate-determining step using the model, the ratio of the net rate to the forward rate for each step was calculated and revealed if a step was quasi-equilibrated or not. It was found that at all times and under all conditions studied, this ratio was equal to one for Step 4 (Fig. 2a). The transformation of **styOMn$_r$** to **styOMn** therefore constituted the rate-determining step. This result agrees with the hypothesis of Collman and coworkers that the rate-determining step involves oxygen transfer to the olefin [17,22].

The microkinetic model is a comprehensive description of the kinetics of this system, but it can be valuable to also capture the kinetics in the form of an analytical rate expression to see the effect of the rate parameters and concentrations of different species more directly. An analytical expression was derived based on the assumption that Step 4 was the rate-determining step and by applying the pseudo-steady state hypothesis to all intermediates, and the result is

$$r = \frac{k_{f1}k_{f2}k_{f3}k_{f4}[sty][PhIO][Mn]^2}{\alpha\{(k_{f3}/K_3) + k_{f4}[Mn]\}\left\{k_{f2}[sty] + (k_{f8} + k_{f9})[Mn] - \frac{k_{f2}(k_{f2}/K_2)[sty]}{\alpha}\right\}}$$

$$\alpha = k_{f2}/K_2 + k_{f3} - \frac{k_{f3}(k_{f3}/K_3)}{(k_{f3}/K_3) + k_{f4}[Mn]} \quad (5)$$

where Mn = MnDPyP and sty = styrene. Comparison of the rates determined from the appearance of the products in the model and calculated from the analytical expression in Eq. (5) confirmed that it accurately describes the kinetics at all times and under all conditions studied. It is interesting that the rate expression has the basic form of a Michaelis–Menten rate expression, but it clearly has a more complicated dependence on the concentrations of different species and depends strongly on the concentration of catalyst as a function of time.

This rate expression demonstrates that reaction orders with respect to styrene and to MnDPyP can vary from 0 to 1 and from 0 to 2, respectively, depending on the nature of the dominant terms in the denominator. To explore this order dependence in more detail, the microkinetic model was used to determine the reaction order in styrene at a reaction time of 2 min. The initial styrene concentration was varied from 1×10^{-6} M to 10 M with the initial MnDPyP and iodosylbenzene concentrations set to 0.2 mM and 0.1 M, respectively. As shown in Fig. 6a, the initial rate was linearly dependent on the initial styrene concentration up to a styrene concentration of 0.05 M. Above this concentration, the initial rate became quickly independent of styrene concentration. The qualitative shape of the curve agrees with the Michaelis–Menten mechanism proposed in the literature and with the analytical rate law given in Eq. (5).

The reaction order in MnDPyP was found to vary over the range of concentrations modeled, which contrasts with the simple Michaelis–Menten mechanism in which the reaction order in catalyst is always one. The reaction order in MnDPyP was calculated over the range of initial MnDPyP concentrations from 1.0×10^{-9} mM to 10.0 mM with initial styrene and iodosylbenzene concentrations set to 0.1 M. Analysis of the model results gave a reaction order in MnDPyP of 2.0 below the initial MnDPyP concentration of 0.3 μM (Fig. 6b). This reaction order in the catalyst has not been found in experimental studies to date because such low initial catalyst concentrations have not been studied. Between initial MnDPyP concentrations of 0.3 μM and 1.0 mM, the reaction

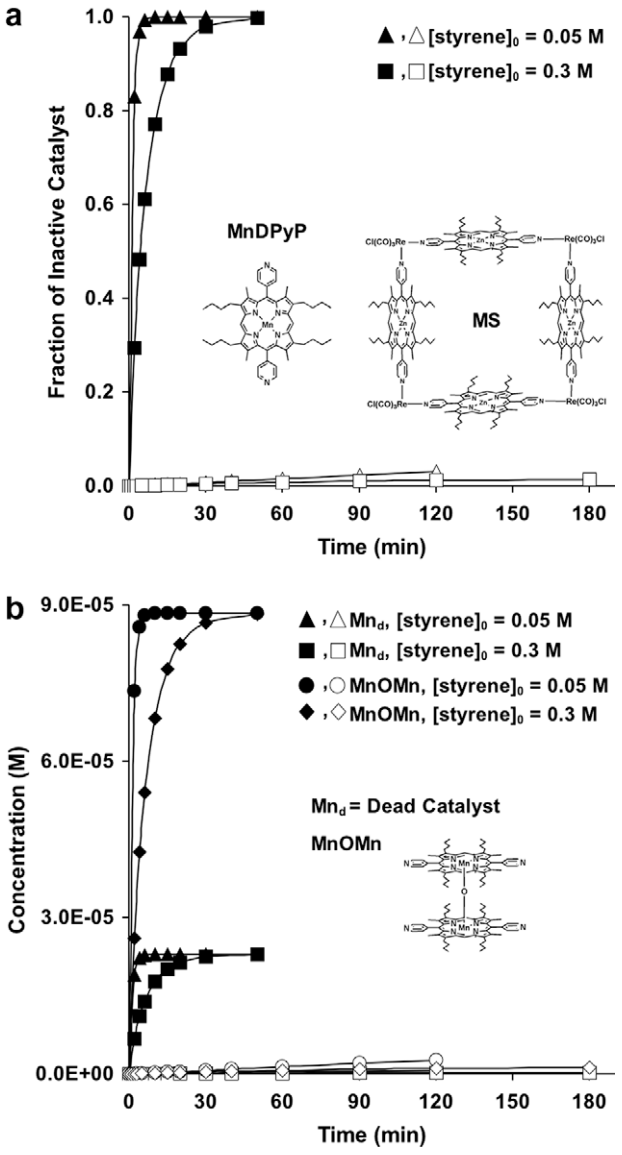

Fig. 5. (a) Fraction of MnDPyP in μ-oxo dimer or deactivated form and (b) concentration of inactive catalyst species (structures shown in the inset) as a function of time for various initial styrene concentrations with $[MnDPyP]_0$ = 0.2 mM and $[iodosylbenzene]_0$ = 0.1 M. Filled symbols denote model results for the MnDPyP system, and open symbols show model results for the [MnDPyP·MS] system with $[MS]_0$ = 0.7 mM. MnDPyP and MS structures are shown in the inset in (a).

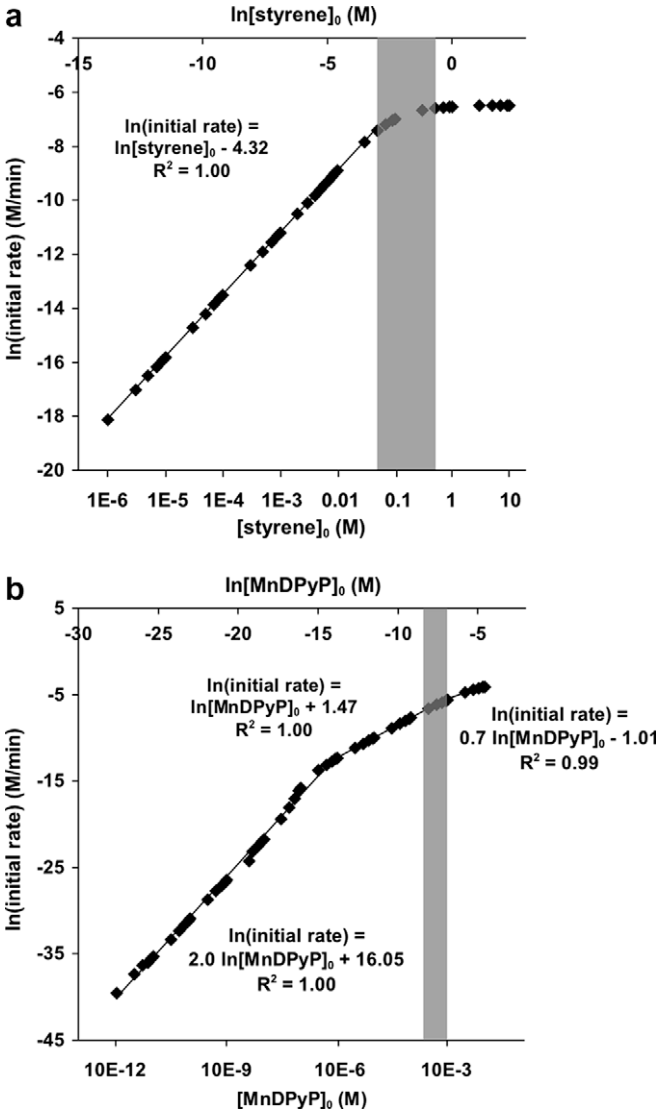

Fig. 6. Dependence of initial rates on (a) initial styrene concentration with $[MnDPyP]_0$ = 0.2 mM at t = 2 min and (b) initial MnDPyP concentration with $[styrene]_0$ = 0.1 M at t = 2 min. In all cases, $[iodosylbenzene]_0$ = 0.1 M. Model results are represented with symbols. The shaded region represents the initial concentrations studied experimentally. Linear fits are shown for different concentration ranges of MnDPyP to show clearly how the reaction order with respect to catalyst changes as the concentration varies.

order was determined to be 1.0 in MnDPyP. This finding agrees with numerous studies in the literature that find a first-order dependence [17–22]. Above an initial MnDPyP concentration of 1.0 mM, the reaction order in MnDPyP decreased to 0.7 in the range studied. A decrease in catalyst reaction order was observed by Nolte and coworkers [4,5], who suggested that the change in the reaction order was a result of μ-oxo dimerization. Investigation of the dominant terms in the denominator of Eq. (5) explained the calculated decrease in the reaction order. At very low MnDPyP concentrations, the terms with MnDPyP dependence were negligible, giving a reaction order of two. When the reaction order was one, the dominant terms included styrene and/or MnDPyP concentrations. At higher MnDPyP concentrations, a term with a second-order dependence on MnDPyP started to become more dominant in the denominator, effecting a reaction order less than one. This term comes from a combination of the three steps with a second-order dependence on MnDPyP (Steps 4, 8, and 9 in Fig. 2a). These results indicate the advantage of using a microkinetic model to capture and explain experimental data under all conditions and at all times. Although a compact rate form captures the data, it is still necessary to know how the MnDPyP concentration varies with time, which was provided directly by the microkinetic model with the inclusion of explicit intermediates and deactivation steps (Steps 8 and 9 in Fig. 2a). In addition, the analytical rate expression was derived based on the fact that Step 4 was rate-determining, which was also the information provided directly by the microkinetic model. These results demonstrate that the simplified Michaelis–Menten mechanism that does not take catalyst deactivation into account is only valid at short reaction times before deactivation becomes significant.

3.2. MnTPP

After developing the mechanism shown in Fig. 2a for the MnDPyP system, the mechanism was used to model the MnTPP

system. The optimized rate parameters for the MnTPP system can be found in Table 3. The sum of squared error was 1.75×10^{-2} M^2 for the optimal fit of the MnTPP data to the microkinetic model shown in Fig. 2a. Parity plots of the styrene and styrene oxide and phenylacetaldehyde concentrations (Fig. 7) demonstrate the reasonable quality of the fit against all 324 data points that were measured experimentally. In particular, the general trends are captured, but at lower catalyst concentrations, the model does not capture the time dependence of the styrene oxide concentration as well as it did for the MnDPyP system (see Supplementary material). This is in part due to the weighting scheme used, which weighted higher concentrations slightly more heavily during regression. Generally, the best agreement between the experiment and the model was obtained at intermediate styrene and MnTPP concentrations (see Supplementary material). Experimentally, the selectivity to epoxide of the MnTPP system at all times and under all conditions studied was found to be somewhat higher than the MnDPyP system (80% vs. 70%). The model captured this difference in selectivity, calculating 84% selectivity for MnTPP compared to the 70% selectivity calculated for MnDPyP.

Deactivation was found to be significant in the MnTPP system as well. Under the experimental conditions studied here, deactivation was significant at times less than 10 min where initial rates are typically measured experimentally (see Supplementary material). The fraction of deactivated catalyst increased with increasing initial catalyst concentration and with decreasing initial styrene concentration. In contrast to the MnDPyP system, essentially all of the inactive catalyst is in the form of μ-oxo dimer at all conditions studied (see Supplementary material). This difference came from the fact that the optimized rate constant for the formation of dead catalyst (Step 9 in Fig. 2a) was ten orders of magnitude higher for the MnDPyP system than for the MnTPP system, while the optimized rate constants and equilibrium constants for the dimerization step (Step 8) were similar for both systems (see Tables 2 and 3). It should be noted that the model tended to overpredict product concentrations at low initial MnTPP and styrene concentrations. The deactivation in the MnTPP system may have therefore been faster than predicted by the model. For the MnTPP system, the deactivation still was significant enough to prevent the simple Michaelis–Menten mechanism from applying at all reaction times.

3.3. [MnDPyP·MS]

To investigate the effect of encapsulation of MnDPyP in molecular squares, the reaction was modeled as a combination of the catalysis by non-encapsulated MnDPyP (Fig. 2a) and the catalysis by encapsulated catalyst (Fig. 2b). The parameters for catalysis by non-encapsulated MnDPyP were fixed at their values given in Table 2, and only the parameters governing catalysis by the encapsulated species were fit. The optimized parameters for the catalysis occurring through encapsulated MnDPyP are given in Table 4. Good agreement between the model and the experimental data was achieved, with a best sum of squared error of 5.55×10^{-2} M^2. Concentration profiles for all styrene oxide data collected are compared to the calculated concentration profiles shown in Fig. 8. Comparison of the experimental and calculated concentration profiles for phenylacetaldehyde can be found in Supplementary material. For the initial MnDPyP concentrations equal to 0.2 mM (shown in Fig. 8a) or initial styrene concentrations of 0.05 M (shown in Fig. 8b and c), the model results at early reaction times underpredict the experimental concentrations of products, while the agreement is reasonable for long reaction times, suggesting that the deactivation kinetics under these conditions are not being precisely captured by the model. The model overpredicts the concentrations of products at short times when the initial MnDPyP concentration is 0.05 mM. For initial MnDPyP concentrations greater than 0.2 mM or initial styrene concentrations greater than 0.05 M, the model does an excellent job capturing the experimental data at all reaction times. The model captured the selectivity of the [MnDPyP·MS] system observed experimentally (64% vs. 66%).

Encapsulation of MnDPyP in molecular squares increases the stability of the catalyst [15]. To show the enhanced stability, an experiment was carried out where the reaction ran to 100% conversion with respect to the limiting reactant (iodosylbenzene). More oxidant was added after 90 min, and the reaction again ran to completion within another 90 min (see Supplementary material). The model captured the enhanced stability as shown in Fig. 5. In the absence of the molecular squares, the MnDPyP catalyst quickly deactivated through the formation of the μ-oxo dimer and dead catalyst (Steps 8 and 9 in Fig. 2a), which accounted for almost all of the catalyst. In the [MnDPyP·MS] system, however, the formation of these species was suppressed because most of the active MnDPyP was

Table 3
Rate constants and equilibrium constants for the reaction mechanism shown in Fig. 2. Comparison of parameters as obtained with the QM/MM method and after their optimization against experimental data is provided for the MnTPP system. Mn = MnTPP; PhIO = iodosylbenzene; OMn = TPPMnO; styOMn$_1$ = loosely bound reactant; styOMn$_r$ = radical intermediate; styOMn = fully formed product complex; styoxMn$_1$ = loosely bound product; styox = styrene oxide; pa = phenylacetaldehyde; MnOMn = μ-oxo (porphyrin)Mn dimer; and Mn$_d$ = dead catalyst. Limits for the optimizations when theoretical values were available: $K_{QM/MM}$ (or $k_{QM/MM}$) × 425 (upper limit) and $K_{QM/MM}$ (or $k_{QM/MM}$) × 0.002 (lower limit). This corresponds to ±15 kJ/mol in ΔG or $\Delta G^{\neq}$.

Step	Reaction and rate equation	QM/MM initial guesses	Optimized parameters
1	Mn + PhIO ↔ OMn + PhI		$k_{f1} = 4.19 \times 10^1$ M^{-1} s^{-1}
	$r_1 = k_{f1}$[Mn][PhIO] − k_{r1}[OMn][PhI]		$k_{r1} = 8.30 \times 10^3$ M^{-1} s^{-1}
2	OMn + sty ↔ styOMn$_l$		$k_{f2} = 1.42 \times 10^9$ M^{-1} s^{-1}
	$r_2 = k_{f2}$[OMn][sty] − k_{f2}/K_2[styMnO$_l$]	$K_2 = 1.71 \times 10^1$ M^{-1}	$K_2 = 4.56 \times 10^1$ M^{-1}
3	styOMn$_l$ ↔ styOMn$_r$	$k_{f3} = 4.68 \times 10^2$ s^{-1}	$k_{f3} = 1.98 \times 10^5$ s^{-1}
	$r_3 = k_{f3}$[styOMn$_l$] − k_{f3}/K_3[styOMn$_r$]	$K_3 = 3.64 \times 10^{-4}$	$K_3 = 1.55 \times 10^{-1}$
4	styOMn$_r$ + Mn ↔ styOMn + Mn	$k_{f4} = 3.84 \times 10^9$ M^{-1} s^{-1}	$k_{f4} = 2.78 \times 10^8$ M^{-1} s^{-1}
	$r_4 = k_{f4}$[styOMn$_r$][Mn] − k_{f4}/K_4[styOMn][Mn]	$K_4 = 1.06 \times 10^5$	$K_4 = 1.19 \times 10^3$
5	styOMn ↔ styoxMn$_l$		$k_{f5} = 3.15 \times 10^{-1}$ s^{-1}
	$r_5 = k_{f5}$[styOMn] − k_{f5}/K_5[styoxMn$_l$]	$K_5 = 2.04 \times 10^9$	$K_5 = 8.67 \times 10^{11}$
6	styoxMn$_l$ ↔ Mn + styox	$k_{f6} = 1.76 \times 10^{11}$ s^{-1}	$k_{f6} = 7.45 \times 10^{13}$ s^{-1}
	$r_6 = k_{f6}$[styoxMn$_l$] − k_{f6}/K_6[Mn][styox]	$K_6 = 1.30 \times 10^{-3}$ M	$K_6 = 5.53 \times 10^{-1}$ M
7	styOMn ↔ Mn + pa	$K_7 = 3.44 \times 10^{29}$ M	$k_{f7} = 6.21 \times 10^{-2}$ s^{-1}
	$r_7 = k_{f7}$[styOMn] − k_{f7}/K_7[Mn][pa]		$K_7 = 1.40 \times 10^{27}$ M
8	Mn + OMn ↔ MnOMn		$k_{f8} = 4.55 \times 10^5$ M^{-1} s^{-1}
	$r_8 = k_{f8}$[Mn][OMn] − k_{f8}/K_8[MnOMn]	$K_8 = 1.24 \times 10^{19}$ M^{-1}	$K_8 = 2.92 \times 10^{16}$ M^{-1}
9	Mn + OMn → Mn$_d$ + Mn		$k_{f9} = 1.00 \times 10^{-5}$ M^{-1} s^{-1}
	$r_9 = k_{f9}$[Mn][OMn]		

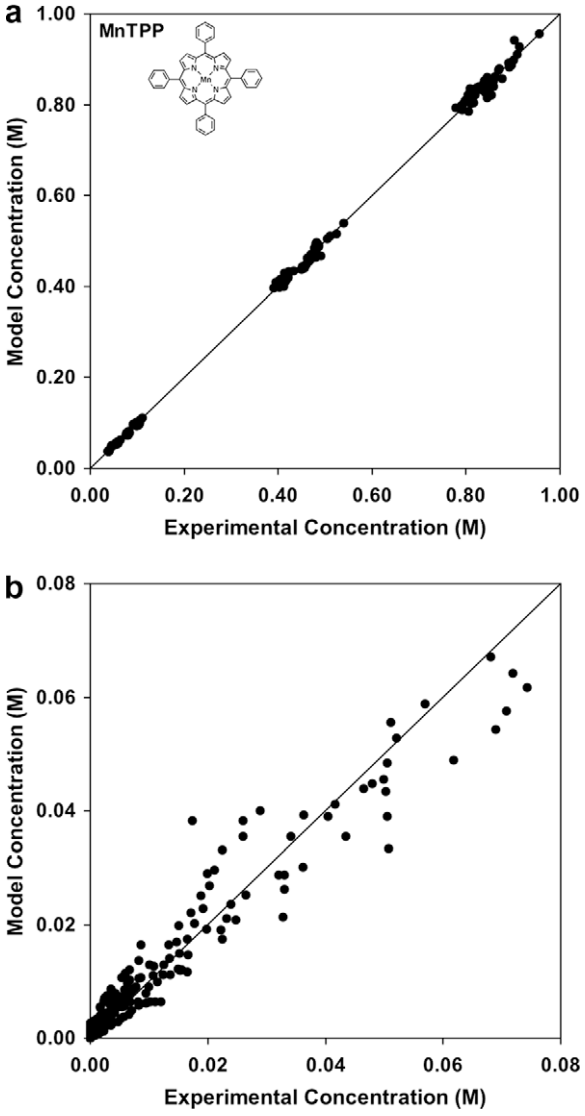

Fig. 7. Parity plots of (a) styrene and (b) styrene oxide and phenylacetaldehyde concentrations for the MnTPP (structure shown in the inset) system.

Table 4
Optimized rate constants and equilibrium constants for the reaction mechanism shown in Fig. 2b for the [MnDPyP·MS] system. MnMS = encapsulated MnDPyP catalyst; OMnMS = encapsulated DPyPMnO; styOMn$_r$MS = encapsulated radical intermediate; and styOMnMS = encapsulated product complex. The value of K_b was fixed at 1.0×10^6 M^{-1} [34].

Step	Reaction and rate equation	Optimized parameters
1	Mn + MS ↔ MnMS	$k_{f1} = 1.66 \times 10^7$ M^{-1} s^{-1}
	$r_1 = k_{f1}$[Mn][MS] − k_{f1}/K_b[MnMS]	
2	MnMS + PhIO ↔ OMnMS + PhI	$k_{f2} = 2.36$ M^{-1} s^{-1}
	$r_2 = k_{f2}$[MnMS][PhIO] − k_{r2}[OMnMS][PhI]	$k_{r2} = 1.00 \times 10^{-5}$ M^{-1} s^{-1}
3	OMnMS + sty ↔ styOMn$_r$MS	$k_{f3} = 5.66 \times 10^1$ M^{-1} s^{-1}
	$r_3 = k_{f3}$[OMnMS][sty] − k_{r3}[styOMn$_r$MS]	$k_{r3} = 4.41 \times 10^8$ s^{-1}
4	styOMn$_r$MS ↔ styOMnMS	$k_{f4} = 4.95 \times 10^6$ s^{-1}
	$r_4 = k_{f4}$[styOMn$_r$MS] − k_{r4}[styOMnMS]	$k_{r4} = 1.00 \times 10^{-5}$ s^{-1}
5	styOMnMS ↔ MnMS + styox	$k_{f5} = 5.59 \times 10^9$ s^{-1}
	$r_5 = k_{f5}$[styOMnMS] − k_{r5}[MnMS][styox]	$k_{r5} = 2.73 \times 10^2$ M^{-1} s^{-1}
6	styOMnMS ↔ MnMS + pa	$k_{f6} = 5.13 \times 10^9$ s^{-1}
	$r_6 = k_{f6}$[styOMnMS] − k_{r6}[MnMS][pa]	$k_{r6} = 4.53 \times 10^2$ M^{-1} s^{-1}

encapsulated in the molecular squares. The concentration of active encapsulated MnDPyP species was at least one order of magnitude higher than that of the active MnDPyP species in solution at high

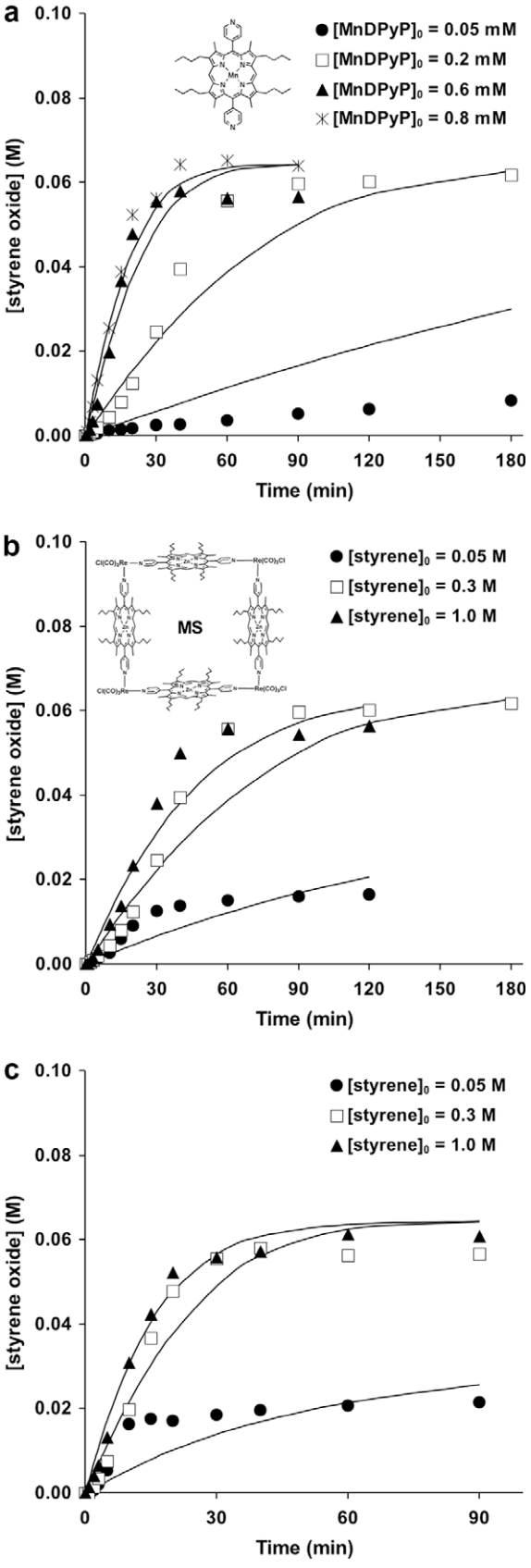

Fig. 8. Styrene oxide concentration profiles for (a) various initial MnDPyP (structure shown in the inset) concentrations with [styrene]$_0$ = 0.3 M, and for various initial styrene concentrations with (b) [MnDPyP]$_0$ = 0.2 mM and (c) [MnDPyP]$_0$ = 0.6 mM. In all cases, [MS]$_0$ = 0.7 mM (structure shown in the inset in (b)), and [iodosylbenzene]$_0$ = 0.1 M. Symbols represent experimental data, and microkinetic model results are represented with lines.

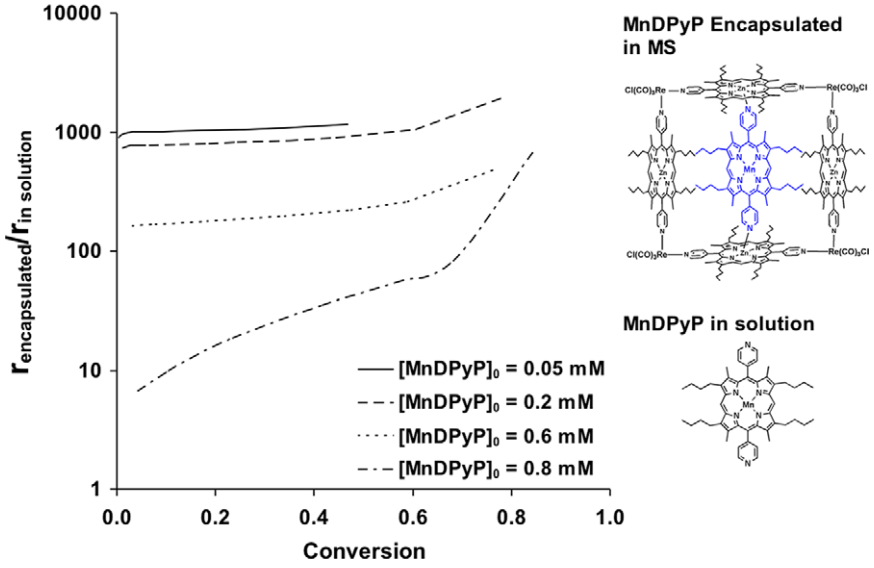

Fig. 9. Ratio of the net rate of epoxide formation by encapsulated MnDPyP to the net rate of epoxide formation by MnDPyP in solution (structures shown in the inset). $[styrene]_0$ = 0.3 M, $[MS]_0$ = 0.7 mM, $[iodosylbenzene]_0$ = 0.1 M.

catalyst concentrations and was 2–3 orders of magnitude higher at lower catalyst concentrations.

The microkinetic model also provided insight into where the catalysis was occurring in the system combining non-encapsulated MnDPyP and [MnDPyP·MS]. An investigation of the ratio of the net rate of epoxide formation by the encapsulated (porphyrin)Mn to that by the free catalyst in solution showed that the net rate of epoxide formation by encapsulated catalyst was on the order of 10^3 faster for various initial styrene concentrations when the initial MnDPyP concentration was 0.2 mM and the concentration of MS was 0.7 mM. This ratio stayed constant regardless of the initial styrene concentration. As shown in Fig. 9, the ratio of the net rate of epoxide formation by encapsulated catalyst to that by the free catalyst depended strongly on the ratio of MnDPyP to molecular squares. As the concentration of MnDPyP was increased at a constant concentration of MS, the epoxidation rate of the free catalyst became more significant relative to the epoxidation rate of the encapsulated catalyst. The ratio of the net rates of epoxide formation by encapsulated and non-encapsulated catalysts decreased from 10^3 to 10^1 as the ratio of MnDPyP to MS increased from 0.07 to 1.1. These results demonstrate that not only do MS serve as a reservoir of catalyst, but they also encapsulate species that actively participate in the epoxidation reaction.

4. Conclusions

Combining kinetic experiments with microkinetic modeling allowed the formulation of a detailed mechanism of epoxidation catalysis by (porphyrin)Mn. The mechanism includes deactivation channels and a series of stable intermediates identified by QM/MM calculations [25]. The proposed mechanism showed good agreement with experimental data for kinetic studies using MnDPyP and MnTPP over a wide range of concentrations and reaction times.

With the microkinetic model, insight into the reaction kinetics was gained that could not be easily obtained with an experiment alone. While the model was able to capture the change in reaction order in styrene observed experimentally by several groups [17–20,22] for both the MnTPP and MnDPyP systems, it showed that simple Michaelis–Menten kinetics do not always capture the reaction order in the catalyst. In particular, high initial catalyst concentrations resulted in reaction orders less than one. The model illustrated the significance of deactivation as most of the catalyst was in μ-oxo dimer form or dead within time scales that would typically be used to determine the initial rates experimentally. The consequence of deactivation is that the simple Michaelis–Menten rate law cannot capture kinetic data at long reaction times.

It was also possible to explain the role of molecular squares in the epoxidation catalysis with the microkinetic model. In particular, the molecular squares prevented deactivation of the MnDPyP catalyst, and the encapsulated porphyrins played a significant role in the catalysis with net rates of epoxide formation one to three orders of magnitude larger than the net rate of epoxide formation by the free catalyst.

Acknowledgments

This research is supported by the National Science Foundation (CTS-0507013), the Chemical Sciences, Geosciences, and Biosciences Division, Office of Basic Energy Sciences, U.S. Department of Energy (DE-FG02-03ER15457), the National Defense Science and Engineering Graduate Fellowship Program (GAEO), and the Illinois Minority Graduate Incentive Program (MCC). The authors thank Professor Joseph T. Hupp for helpful discussions.

Appendix A. Supplementary material

Supplementary data associated with this article can be found, in the online version, at doi:10.1016/j.jcat.2009.06.003.

References

[1] J.T. Groves, W.J. Kruper, R.C. Haushalter, J. Am. Chem. Soc. 102 (1980) 6375.
[2] E.N. Jacobsen, in: G. Wilkinson, F.G.A. Stone, E.W. Abel, L.S. Hegedus (Eds.), Comprehensive Organometallic Chemistry II, Pergamon, New York, 1995, p. 1097.
[3] J.A.S.J. Razenberg, A.W. Van der Made, J.W.H. Smeets, R.J.M. Nolte, J. Mol. Catal. 31 (1985) 271.
[4] R.J.M. Nolte, J.A.S.J. Razenberg, R. Schuurman, J. Am. Chem. Soc. 108 (1986) 2751.
[5] J.A.S.J. Razenberg, R.J.M. Nolte, W. Drenth, J. Chem. Soc., Chem. Commun. (1986) 277.
[6] M.C. Feiters, A.E. Rowan, R.J.M. Nolte, Chem. Soc. Rev. 29 (2000) 375.
[7] F.G. Doro, J.R.L. Smith, A.G. Ferreira, M.D. Assis, J. Mol. Catal. A: Chem. 164 (2000) 97.
[8] P.E.F. Neys, A. Severeyns, I.F.J. Vankelecom, E. Ceulemans, W. Dehaen, P.A. Jacobs, J. Mol. Catal. A: Chem. 144 (1999) 373.
[9] H.C. Sacco, Y. Iamamoto, J.R.L. Smith, J. Chem. Soc., Perkin Trans. 2 (2001) 181.

[10] J.P. Collman, X. Zhang, V.J. Lee, E.S. Uffelman, J.I. Brauman, Science 261 (1993) 1404.
[11] S.T. Nguyen, D.L. Gin, J.T. Hupp, X. Zhang, Proc. Natl. Acad. Sci. USA 98 (2001) 11849.
[12] S. Bélanger, J.T. Hupp, Angew. Chem., Int. Ed. 38 (1999) 2222.
[13] J.T. Hupp, in: E. Alessio (Ed.), Structure and Bonding, 2006, p. 145.
[14] S.J. Lee, J.T. Hupp, Coord. Chem. Rev. 250 (2006) 1710.
[15] M.L. Merlau, M. del Pilar Mejia, S.T. Nguyen, J.T. Hupp, Angew. Chem., Int. Ed. 40 (2001) 4239.
[16] J.A. Dumesic, D.F. Rudd, L.M. Aparicio, J.E. Rekoske, A.A. Treviño, The Microkinetics of Heterogeneous Catalysis, American Chemical Society, USA, 1993.
[17] J.P. Collman, J.I. Brauman, B. Meunier, T. Hayashi, T. Kodadek, S.A. Raybuck, J. Am. Chem. Soc. 107 (1985) 2000.
[18] B. Meunier, M.-E. De Carvalho, A. Robert, J. Mol. Catal. 41 (1987) 185.
[19] H. Amatsu, T.K. Miyamoto, Y. Sasaki, Bull. Chem. Soc. Jpn. 61 (1988) 3193.
[20] J.P. Collman, J.I. Brauman, P.D. Hampton, H. Tanaka, D.S. Bohle, R.T. Hembre, J. Am. Chem. Soc. 112 (1990) 7980.
[21] S. Banfi, M. Cavazzini, G. Pozzi, S.V. Barkanova, O.L. Kaliya, J. Chem. Soc., Perkin Trans. 2 (2000) 871.
[22] J.P. Collman, L. Zeng, H.J.H. Wang, A. Lei, J.I. Brauman, Eur. J. Org. Chem. 2006 (2006) 2707.
[23] A.D. Adler, F.R. Longo, F. Kampas, J. Kim, J. Inorg. Nucl. Chem. 32 (1970) 2443.
[24] R.V. Slone, J.T. Hupp, Inorg. Chem. 36 (1997) 5422.
[25] M.C. Curet-Arana, R.Q. Snurr, L.J. Broadbelt, in: T. Oyama (Ed.), Mechanisms in Homogeneous and Heterogeneous Epoxidation Catalysis, Elsevier, Amsterdam, 2008, p. 471.
[26] M.C. Curet-Arana, G.A. Emberger, L.J. Broadbelt, R.Q. Snurr, J. Mol. Catal. A: Chem. 285 (2008) 120.
[27] J.T. Groves, J. Lee, S.S. Marla, J. Am. Chem. Soc. 119 (1997) 6269.
[28] N. Jin, J.L. Bourassa, S.C. Tizio, J.T. Groves, Angew. Chem., Int. Ed. 39 (2000) 3849.
[29] N. Jin, J.T. Groves, J. Am. Chem. Soc. 121 (1999) 2923.
[30] R. Zhang, J.H. Horner, M. Newcomb, J. Am. Chem. Soc. 127 (2005) 6573.
[31] W.J. Song, M.S. Seo, S.D. George, T. Ohta, R. Song, M.-J. Kang, T. Tosha, T. Kitagawa, E.I. Solomon, W. Nam, J. Am. Chem. Soc. 129 (2007) 1268.
[32] D. Feichtinger, D.A. Plattner, Angew. Chem., Int. Ed. 36 (1997) 1718.
[33] D. Feichtinger, D.A. Plattner, Chem. Eur. J. 7 (2001) 591.
[34] J.T. Groves, M.K. Stern, J. Am. Chem. Soc. 109 (1987) 3812.
[35] J.T. Groves, M.K. Stern, J. Am. Chem. Soc. 110 (1988) 8628.
[36] R.D. Arasasingham, G.-X. He, T.C. Bruice, J. Am. Chem. Soc. 115 (1993) 7985.
[37] L. Cavallo, H. Jacobsen, Angew. Chem., Int. Ed. 39 (2000) 589.
[38] L. Cavallo, H. Jacobsen, J. Phys. Chem. A 107 (2003) 5466.
[39] C. Linde, B. Åkermark, P.O. Norrby, M. Svensson, J. Am. Chem. Soc. 121 (1999) 5083.
[40] M. Caracotsios, W.E. Stewart, Comput. Chem. Eng. 19 (1995) 1019.
[41] J.O. Hirschfelder, E. Wigner, J. Chem. Phys. 7 (1939) 616.
[42] B. Hammer, L.B. Hansen, J.K. Norskov, Phys. Rev. B: Condens. Matter Mater. Phys. 59 (1999) 7413.
[43] K. Honkala, A. Hellman, I.N. Remediakis, A. Logadottir, A. Carlsson, S. Dahl, C.H. Christensen, J.K. Norskov, Science 307 (2005) 555.
[44] D.E. Goldberg, Genetic Algorithms in Search, Optimization, and Machine Learning, Addison-Wesley, USA, 1989.
[45] W.E. Stewart, M. Caracotsios, J.P. Sorensen, AIChE J. 38 (1992) 641.
[46] J.W. Moore, R.G. Pearson, Kinetics and Mechanism, John Wiley & Sons, New York, 1981.
[47] D. Majumder, Multiscale Modeling for Materials Design: Molecular Square Catalysts, Ph.D. Thesis, Northwestern University, Evanston, IL, 2006.
[48] I.V. Zakharov, Y.V. Kumpan, Kinet. Catal. 34 (1993) 922.
[49] M.F. Powell, E.F. Pai, T.C. Bruice, J. Am. Chem. Soc. 106 (1984) 3277.